CO6-1 Study of DNA DSB end structure induced by ionizing radiation

K. Akamatsu[1], N. Shikazono[1] and T. Saito[2]

[1]*Radiation DNA Damage Research Group, Kansai Photon Science Institute, National Institutes for Quantum and Radiological Science and Technology (QST)*

[2]*KURNS, Kyoto University*

INTRODUCTION:

Clustered damage site, that is a DNA region with multiple lesions within a few helical turns, is believed to hardly be repaired. However, chemical and spatial details of them are not known. We are developing a methodology for studying structural feature of DNA DSB end and affinity between the DSB end and a repair protein. We have tried to irradiate gamma-rays and iron ion beam with LET of ~0.2 and ~200 keV/μm, respectively, to pUC19 in a cell-mimetic buffered solution. As a result, we found that these ions tend to produce *direct* DSB (except for a DSB by sequentially-produced opposed close SSBs) compared with ^{60}Co γ-rays. We will isolate linear pUC19 with DSB ends and study how a repair protein recognize and process a DSB end.

EXPERIMENTS:

●*Sample preparation and irradiation*

The plasmid DNA (pUC19, 2686bp) was used. The DNA was dissolved to be 0.1 g/L in 0.2 M Tris-HCl buffer (pH 7.5) which is a cell-mimetic condition in relation to radical scavenging capacity. Twenty microliters of the DNA solution was transferred to a micro chamber (20-μL size), and was irradiated with Fe ion beam (LET: ~200 keV/μm; HIMAC QST) and ^{60}Co γ-rays (LET: ~0.2 keV/μm; KURNS Kyoto University) as a standard radiation source. The irradiated DNA sample was purified by ethanol precipitation and was dried in vacuum, followed by being kept at -20ºC until use.

●*Agarose gel electrophoresis of irradiated DNA*

The dry irradiated DNA samples were dissolved to TE buffer (~2g/L). The electrophoresis was performed for 4h, 70V at 4ºC. The gel was stained by ethidium bromide (EtBr). The different DNA forms separated (supercoiled (sc), open circular (oc), and linear (L) form) were quantified by a gel imager (Pharos FX, BioRad).

●*Large-amount Isolation of lin fraction using agarose electrophoresis*

We have constructed a protocol for collecting large amount of lin fraction using general agarose electrophoresis (1% agarose in 0.5xTBE, 25V, 18h) pUC19/SmaI was used as a marker. EtBr staining was performed only to the marker lane. L fraction was collected from L-containing gel fragments by electroelution (D-Tube Dialyzer, Maxi, Novagen), followed by buffer exchange to TE (Amicon Ultra-4, Millipore). The collected L fraction will be used for several biochemical and physicochemical analysis.

RESULTS:

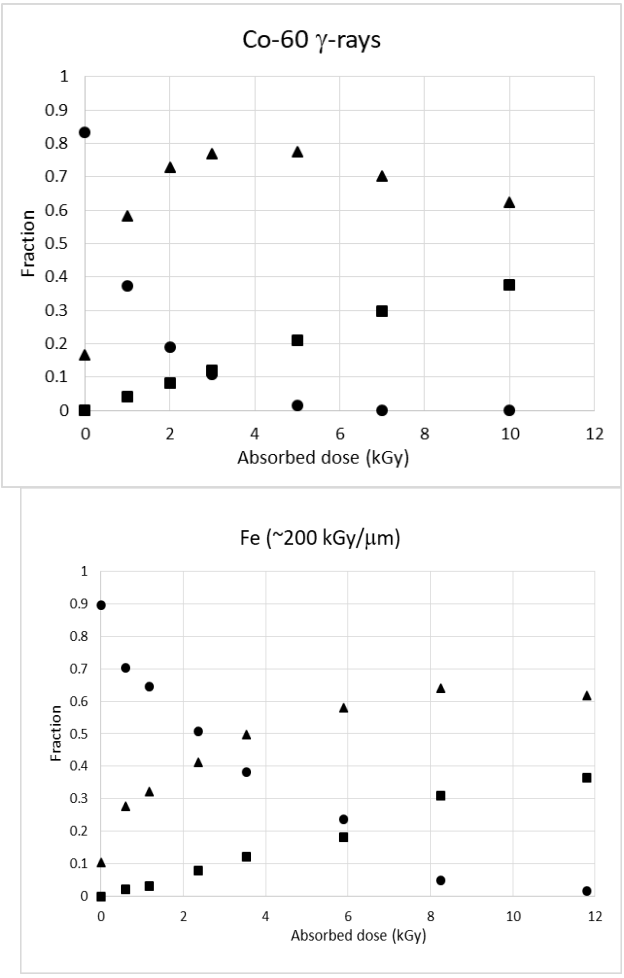

Fig. 1. Relationship between absorbed dose and DNA fractions (●: sc, ▲: oc, ■: L) for ^{60}Co γ-rays (upper panel) and Fe ion beam (lower panel).

The fraction maximum of L for ^{60}Co γ-rays is ~0.8, whereas that for Fe beam dose is ~0.6, suggesting that Fe beam is likely to induce *direct* dsb formation from sc form compared with the γ-rays. The yield ratios of dsb to total strand breaks for γ and Fe are calculated to be 0.067 and 0.17, respectively, according to Cowan's theory [1].

What is a *direct* dsb? How difference are shown between a *direct* dsb and successive dsb (by ssb + ssb)? How is a *direct* dsb repaired? These are our issues to be solved.

REFERENCES:

[1] R.Cowan, *et al.,* J.Theor.Biol. **81** (1987) 229-245.

30001

CO6-2 Oligomeric structures of HspB1 from CHO cell

M. Yohda, K. Ankai, R. Inoue[1], K. Morishima[1], N. Sato[1], M. Sugiyama[1]

Department of Biotechnology and Life Science, Tokyo University of Agriculture and Technology
[1]Institute for Integrated Radiation and Nuclear Science, Kyoto University

INTRODUCTION: Small heat shock proteins (sHsps) endow cells with stress tolerance [1]. They bind to partially folded or denatured proteins, thereby preventing irreversible aggregation or promoting correct substrate folding. Various species of sHsps are present in mammals [2]. HspB1, also known as Hsp27, is a ubiquitous sHsp [3]. The sHsps of mammals, which reflect their status as homeotherms, are regulated by phosphorylation. To examine the structure and function of HspB1, we expressed, purified and characterized HspB1 from Chinese hamster (*Cricetulus griseus*) ovary cells (CgHspB1) (Manuscript in preparation). CgHspB1 forms a large oligomeric structure. In dilute conditions, CgHspB1 dissociates into small oligomers at the elevated temperatures. In contrast, dissociation of the oligomer was not observed at the relatively high protein concentrations. The phosphorylation mimic mutant of CgHspB1 with the replacement of Ser15 to Asp (CgHspB1_S15D) exhibited relatively lower oligomer stability and higher ability for protecting thermal aggregation than the wild-type protein. The result clearly showed the correlation between oligomer dissociation with chaperone activity. In this study, we compared the oligomeric structures of CgHspB1 wild type and CgHspB1_S15D by various methods.

EXPERIMENTS: CgHSPB1 variants (CgHspB1_WT, CgHspB1_S15D) were expressed in *E. coli* and purified by anion exchange chromatography with DEAE-TOYOPEARL, anion exchange chromatography with RESOURCE Q and size-exclusion chromatography with Superdex 200. The molecular weights of the oligomers of CgHspB1 variants were analyzed by Size-exclusion chromatography - multiangle light scattering (SEC–MALS) using a multiangle light-scattering detector (MINI DAWN, Wyatt Technology). The oligomeric conformation of CgHspB1 variants were analyzed by small angle X-ray scattering (SAXS) using NANOPIX (Rigaku) and analytical ultracentrifugation (AUC) using XL-1 (Beckman Coulter Diagnostics).

RESULTS: CgHspB1 variants were analyzed by SEC–MALS. The molecular mass of CgHspB1_WT and CgHspB1_S15D were estimated to be about 470 kDa and about 780 kDa, respectively.

Then, they were applied for the analysis by AUC (Fig. 1). The sedimentation velocities were calculated to be 15.1 S (403 kDa) for CgHspB1_WT and 18.2 S (829 kDa) for CgHspB1_S15D. The values well coincide with the molecular mass determined by SEC-MALS.

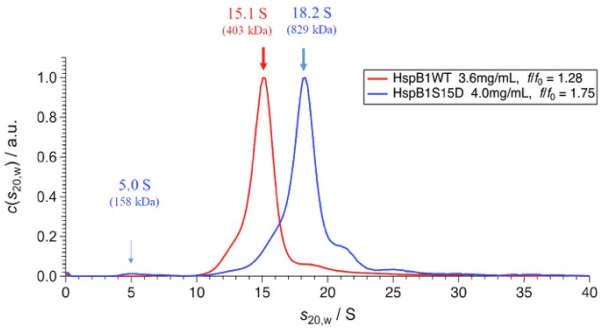

Fig. 1 Analytical centrifugation of CgHspB1 variants

Finally, we have analyzed CgHspB1 variants by SAXS (Fig. 2). *R*g values were calculated to be 58.4 (± 0.6) Å for CgHspB1_WT and 66.9 (± 1.2) Å for CgHspB1_S15D, respectively. SAXS also showed that CgHspB1 changes to the larger oligomeric conformation in the phosphorylated state.

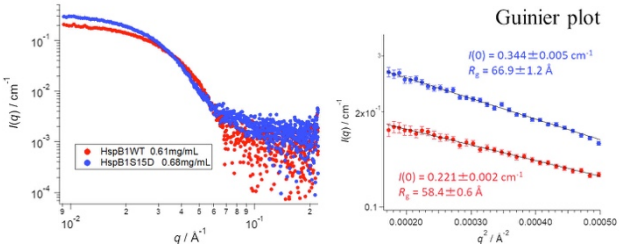

Fig. 2 SAXS profiles of CgHspB1 variants (Left) and the Guinier plots (Right)

Previously, we have shown that the oligomer of CgHspB1_S15S, the phosphorylated mimic mutant, is relatively unstable and dissociates to small oligomers even at the room temperature. In this study, we have shown that the oligomeric structure of CgHspB1_S15S is larger than that of the wild type. Since similar change was observed for CgHspB1_WT at the elevated temperature (Manuscript in preparation), the structure might be the activated conformation of CgHspB1 before dissociation.

REFERENCES:

[1] U. Jakob *et al.,* J. Biol. Chem., 268 (1993) 1517-1520.
[2] C. Garrido *et al.,* Int. J. Biochem. Cell. Biol., 44 (2012) 1588-1592.
[3] A.P. Arrigo., Cell Stress Chaperones., 22 (2017) 517-529.

CO6-3 Effect of ligand Binding on Solution Structure of Multi-domain protein, MurD

H. Nakagawa, T. Saio[1,2], M. Sugiyama[3], R. Inoue[3]

Materials Science Research Center, Japan Atomic Energy Agency

[1]*Graduate School of Chemical Sciences and Engineering, Hokkaido University*

[2]*Department of Chemistry, Faculty of Science, Hokkaido University*

[3]*KURNS, Kyoto University*

INTRODUCTION: In structural biology, precise determination of three-dimensional structures of proteins has been focused, and the structures with an atomic-resolution have given solid platforms to understand their biological functions. Recently, the idea of structural biology has extended beyond the static structural information with atomic resolution, in order to cover more complex and dynamical structures at different levels of space and time resolution. SAXS measurement can observe the solution structure of flexible protein under the physiological conditions [1].

MurD (UDP-N-acetylmuramoylalanine--D-glutamate ligase) is a typical multi-domain protein (Fig.1), which is one of the ATP-driven Mur ligases that are responsible for peptidoglycan biosynthesis. The crysital structure of MurD has been determined, but the ATP-bound form is not detemied.

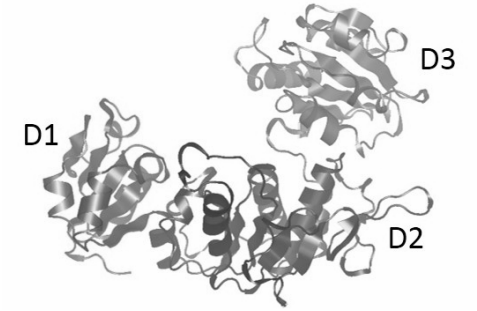

Fig. 1. Multi-domain protein, MurD, which are composed of three domains, D1, D2 and D3.

EXPERIMENTS: MurD were expressed in E. coli strain BL21 (DE3). Small angle X-ray scattering (SAXS) were measured for MurD in ATP-unbound and bound states at the concentration of 5, 10, 20 and 50 mg/ml. The buffer conditions were 20 mM Tris-HCl at pH=7.2. For the sample of ATP-bound state, AMP-PNP and $MgCl_2$ were added at the concentration of 2 mM and 5 mM, respectively. For the sample of Compound1-bound state, Compound1 was added at 3 eq.

RESULTS: SAXS profiles of MurD were successfully obtained for Apo, ATP-bound and Compound1-bound states at 5 mg/mL, where the inter-particle interaction effects were not observed in the profiles. As shown in Fig. 2, SAXS profiles are different among the three samples, indicating the structural change by ATP or Compound1 binding. The previous NMR measurement predicted that the domain orientation of MurD is changed into semi-closed conformation by ATP binding, and closed conformation by Compound1 binding [2]. And our preliminary MD simulation shows that the conformation and fluctuation of MurD domains are changed by ATP- or Compond1-binding, and that these are consistent with the NMR results. The comparison of the SAXS profiles with the results of the NMR and MD simulation are in progress.

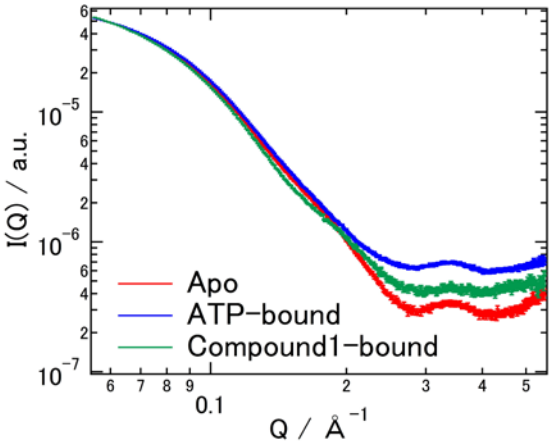

Fig. 2. SAXS profiles in Apo, ATP-bound and Compound1-bound states of MurD at the concentration of 5 mg/ml.

REFERENCES:

[1] J. Trewhella *et al.*, Acta Cryst. **D73** (2017) 710-728.
[2] T. Saio *et al.*, Sci. Rep., **5** (2015) 16685.

CO6-4 Structural characterization of circadian clock potein complexes

H. Yagi, Y. Yunoki, K. Morishima[1], N. Sato[1], R. Inoue[1], and M. Sugiyama[1]

Graduate School of Pharmaceutical Sciences, Nagoya City University,
[1]Institute for Integrated Radiation and Nuclear Science, Kyoto University

INTRODUCTION: The central oscillator that generates the circadian rhythm in the cyanobacterium comprises only three proteins—KaiA, KaiB, and KaiC. Through interactions among these proteins in the presence of ATP, KaiC undergoes phosphorylation and dephosphorylation cycles with the period of 24 h, which proceeds *in vitro* without daylight oscillation, indicating that the internal clock mechanism can be autonomous irrespective of transcriptional and translational feedback systems. Although the formation of several complexes, such as KaiA-KaiC, KaiB-KaiC, and KaiA-KaiB-KaiC oscillated in a circadian manner, their stoichiometry or the detailed structures remains to be elucidated. Herein, in order to understand the oscillation mechanism mediated by the clock protein complex, we characterized the complexes by using analytical ultracentrifugation (AUC) and small angle X-ray scattering (SAXS) analyses. Especially, in this study, we focused on the characterization of KaiA-KaiB-KaiC complex.

EXPERIMENTS: The expression and purification of clock proteins, KaiA, KaiB and KaiC were performed according to methods previously described [1]. SAXS pattern was collected with NANOPIX (Rigaku Corporation, Japan) equipped with HyPix-6000. A Cu Kα line (MicroMAX-007HF) was used as a beam source, which was further focused and collimated with a confocal multilayer mirror (OptiSAXS). The camera length was set to 1.326 m and the range of the scattering vector q was from 0.007 to 0.24 A^{-1}. The AUC experiments were performed using an ProteomeLab XL-I analytical ultracentrifuge (Beckman-Coulter) at 25 °C and an angular velocity of 60,000 rpm. Data were recorded with Rayleigh interference optical system, followed by the analysis with a $c(s)$ distribution of the Lamm equation solutions calculated by the SEDFIT v15.01. The sedimentation coefficient s were converted to the value in water at 20 ºC.

RESULTS: To date, we have reported that KaiB and KaiC formed a complex exclusively in a 6:6 stoichiometry, indicating that KaiB bound to the KaiC hexamer with strong positive cooperativity [1]. Herein we conducted the titration analysis of KaiB-KaiC complex and KaiA for characterization of stoichiometry by SAXS and AUC analyses.

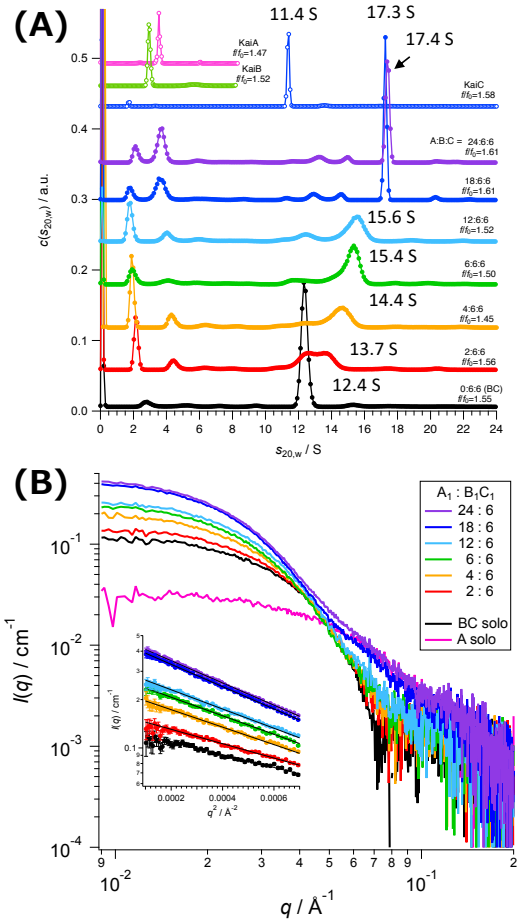

Fig. 1. (A) AUC and (B) SAXS data from titration series with KaiA and KaiBC complex.

The AUC data confirmed that KaiA, KaiB, and KaiC form complexes containing different number of KaiA molecules and form a 12:6:6 complex with a sedimentation coefficient of 17.4 S under the excess amount of KaiA (Fig.1A). The forward scattering $I(0)$ as well as the radius of gyration (Rg) were calculated with the Guinier approximation (Fig.1B). These data also indicated the complex shows the 12:6:6 stoichiometry under the excess amount of KaiA. These data consistent with the model resulting from X-ray crystal structures of KaiB-KaiC 6:6 complex and ternary complex containing KaiA, KaiB, and CI domain of KaiC.

On the basis of our data, we conclude that KaiB-KaiC complex was capable of binding a maximum of 12 KaiA molecules. These findings provide mechanistic insights into the circadian periodicity in cyanobacteria.

REFERENCES:

[1] M. Sugiyama *et al.*, Si. Rep., **6:35567** | (2016).

CO6-5 Sustainable Photoproduction of Medical ^{18}F and ^{99m}Tc Isotopes

T. Takeda, M. Fujiwara[1,2], M. Kurosawa[1], N. Takahashi[1,] M. Tamura[1], T. Kawabata, Y. Fujikawa, K.N. Suzuki, N. Abe[3], T. Kubota[3] and T. Takahashi[3]

Department of Physics, Kyoto University
[1]Research Center for Nuclear Physics, Osaka University
[2]National Institutes for Quantum and Radiological Science and Technology
[3]Institute for Integrated Radiation and Nuclear Science, Kyoto University

INTRODUCTION:

We examined two sustainable methods for producing the medical ^{18}F and ^{99m}Tc isotopes. A new method is proposed for producing medical ^{18}F isotopes as an alternative to the ^{18}F cyclotron production. ^{18}F isotopes are produced via the photoreaction on ^{20}Ne. Natural neon gas is used as a target in the gas recycling flow system. The ^{18}F-FDG radio-pharmaceuticals are obtained by blowing small bubbles of irradiated neon gas in the FDG liquid. Another method is the production of ^{99m}Tc isotopes via the photoreaction on natural MoO_3. In these two methods, both ^{99m}Tc isotopes for the SPECT inspections and ^{18}F isotopes for the PET inspections are sustainably produced using the photoreaction on natural MoO_3 and Ne targets. We have demonstrated the feasibilities of practical usages of these two new methods.

^{18}F EXPERIMENTS:

We used an electron beam from the linear accelerator facility at Institute for Integrated Radiation and Nuclear Science of Kyoto University (KURNS-LINAC) for producing RI from photoreactions. A 40 MeV electron beams with an intensity of 3-9 μA is used to bombard a platinum target with a thickness of 4 mm to generate bremsstrahlung photons for producing ^{18}F via the photoreaction on natural Ne gas.

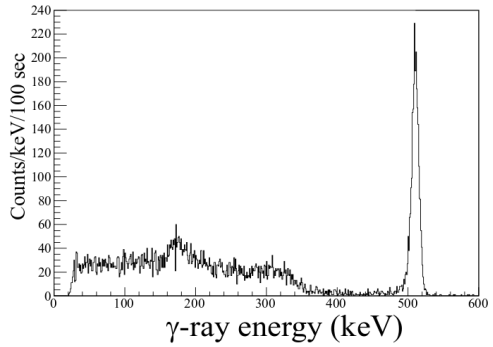

The Ne-gas circulation system has been newly constructed for the present experiment. The irradiation time of bremsstrahlung photons was one hour. The produced ^{18}F isotopes are expected to circulate with Ne gas. When the Ne gas is blow with ^{18}F isotopes in the FDG liquid, ^{18}F isotopes are trapped by FDG, resulting 18F-FDG. The first purpose of the experiment was to examine this principle. Instead of FDG, we used a sodium hydroxide (NaOH) aqueous solution to trap ^{18}F in the first trial.

Figure shows the γ-ray spectrum measured with a CdZnTe detector as a function of the elapsed time in step of 100 second. The decay curve of the 511 keV γ-ray peak is found to be well fitted with a half-life of 110 minutes, demonstrating that the radio-activities trapped in the NaOH water solution are only due to the ^{18}F isotopes. On base of this initial experiment, we have obtained a patent [1].

There are the remaining problems to be solved: One is the trapping efficiency of produced ^{18}F radio-activities in the used gas flow system. We now improve the system to avoid the surface absorption of ^{18}F activities at the inner pipes of the gas flow system. In order to drastically increase the trapping efficiency, we have introduced the SiC ceramic chamber with Teflon coating at inner surface. Another problem is the small yield of ^{11}C with a short half-life of 20.3 minutes, which should be reduced to be as small as possible by replacing the Teflon chamber to SiC chamber. This reduction is also possible by properly collimating the bremsstrahlung photons at the Ne gas target. At present, we are preparing a new paper concerning the ^{18}F production on Ne gas [3].

^{99m}Tc EXPERIMENTS:

Our new paper [2] on the ^{99m}Tc production published in August 2018 has attracted experts of attention. The download amounts to 320 in a half year. In order to refine the project furthermore, a technology to easily extract the ^{99m}Tc isotopes from the radioactivities produced via the (γ,n) reaction on natural Mo are being developed in connection with the noble technologies in materials science.

REFERENCES:

[1] N. Takahashi, Patent Number 6274689 (Japan).
[2] T. Takeda *et al.*, ^{99m}Tc production via the (γ,n) reaction on natural Mo, Journal of Radioanalytical and Nuclear Chemistry (2018) **318**: 811-821.
[3] M. Kurosawa, M. Fujiwara, M. Tamura, N. Takahashi *et al.*, to be submitted to JRNC.

CO6-6 Conformational Characterization of Archaeral Homolog of Proteasome-assembly Chaperone PbaA

M. Yagi-Utsumi, R. Inoue[1], N. Sato[1], M. Sugiyama[1] and K. Kato

Institute for Molecular Science, National Institutes of Natural Sciences
[1]Institute for Integrated Radiation and Nuclear Science, Kyoto University

INTRODUCTION: Recent bioinformatic analyses identified proteasome assembly chaperone-like proteins, PbaA and PbaB, in archaea. PbaB forms a homotetramer and functions as a proteasome activator, whereas PbaA does not interact with the proteasome despite the presence of an apparent C-terminal proteasome activation motif [1, 2]. The C-terminal α6 helices of the PbaB tetramer show tentacle-like structures that project from the core domain, whereas the corresponding C-terminal helical segments of a PbaA pentamer are packed against the core. These structural features may explain the distinct proteasome-binding capabilities of PbaA and PbaB, although the conformational difference may be due to different modes of crystal packing [3]. Interestingly, previous proteome and SAXS-based structural proteomics analyses revealed that PbaA forms a stable complex with an unknown function protein PF0014 [4]. Existence of the putative binding partner protein raised possibilities that it might have some specific role in the PbaA structural design. However, there are no detailed structural information about the protein complex. Thus, we attempted to characterize the structural features of PbaA together with the PF0014 protein by an integrative structural analysis including small-angle X-ray scattering (SAXS).

EXPERIMENTS: The expression and purification of *P. furiosus* PbaA, PbaB and the 20 S proteasome were performed according to methods previously described [1, 2]. SAXS experiments were performed with NANOPIX (Rigaku) at 20°C. X-rays from a high-brilliance point-focused X-ray source (MicroMAX-007HF) were focused and collimated with a confocal multilayer mirror (OptiSAXS) and low parasitic scattering pinhole slits (ClearPinhole). The scattered X-rays were detected using a two-dimensional semiconductor detector (HyPix-6000). The SAXS pattern was converted to a one-dimensional scattering profile, and then standard corrections were applied for initial beam intensity, background scattering and buffer scattering. HS-AFM and EM analyses were also performed.

RESULTS: To obtain information on the overall structure of PbaA/PF0014 complex, we performed HS-AFM and SAXS experiments of PbaA/PF0014 in solution. The HS-AFM data revealed that PbaA/PF0014 complex makes dumbbell-shaped structure in solution and the central pore of PbaA was closed upon complex formation of PF0014. The Ab initio shape modelling from SAXS data (Fig. 1) also demonstrated the dumbbell-shaped structure, in which the estimated radius of gyration (Rg) and the maximum dimension (Dmax) were 55.3±0.1 Å and 178 Å, respectively. Furthermore, using EM and small-angle neutron scattering, we determined the spatial arrangement of PbaA and PF0014 in their dumbbell-shaped complex.

Our study underscores the idea that the functional binding partner of PbaA in archaeal cells is not the proteasome but the PF0014 protein. Although the function of this protein tholos remains unexplored, the structural architecture suggests its capability for molecular encapsulation in archaeal cells.

The unique assembly state of PbaA with PF0014 can provide a new direction to think why this complexity does exist or whether it has some sophisticated novel functional roles in the living system. For example, because of its conformational versatility, PbaA may form different oligomeric structures in response to environmental changes surrounding the organism.

In summary, this study revealed unique structural architectures involving the archaeal homologs of proteasome assembly chaperones, giving new insights into the structural design underlying the dynamic ordering of biomolecules that have internal complexities for the creation of integrated functions.

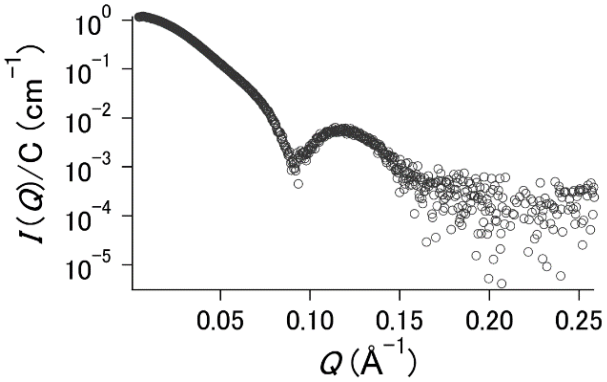

Fig. 1. The SAXS profile of PbaA/PF0014 complex.

REFERENCES:

[1] K. Kumoi *et al.*, PLoS ONE, **8** (2013) e60294.
[2] A. Sikdar *et al.*, Biochem. Biophys. Res. Commun., **453** (2014) 493-497.
[3] M. Yagi-Utsumi *et al.*, Protein Eng. Des. Sel., **31** (2018) 29-36.
[4] Hura, G. L. *et al*. Nat Methods **6** (2009) 606-612.

CO6-7 Time-Resolved Small Angle X-ray Scattering (SAXS) Measurements on the Formation of Insulin B Chain Prefibrillar Intermediates

N. Yamamoto, E. Chatani, R. Inoue[1], K. Morishima[1], and M. Sugiyama[1]

Graduate School of Science, Kobe University
[1]KURNS,Kyoto University

INTRODUCTION: Amyloid fibrils are a kind of protein aggregates associated with a numerous number of diseases. Amyloid fibrils typically exhibit fibrous morphology and β-sheet-rich structure, and the formation of amyloid fibrils typically follows a nucleation-dependent polymerization mechanism. Although a one-step nucleation has widely been accepted as the simplest scheme, a variety of oligomers have been identified in early stages of fibrillation. The oligomers have recently been focused on as an intermediate species involved in the nucleation process as well as molecular species responsible for cytotoxicity [1].

We recently found that prefibrillar intermediates were formed in the early phases of amyloid fibril formation of an insulin-derived peptide (insulin B chain) [2]. In this study, to elucidate the formation mechanisms of the prefibrillar intermediates, we performed time-resolved SAXS measurements of the fibrillation reaction of insulin B chain. Among the wide variety of established analytical techniques stated above, SAXS is one of the most useful approaches to monitor the early events that direct the formation of fibril nuclei [3,4].

EXPERIMENTS: Human insulin was dissolved in 50 mM Tris-HCl, pH8.7. Dithiothreitol was then added to start the reduction of insulin. The solution was kept under 25 °C overnight and a precipitate formed was separated by ultracentrifugation. After rinsed with cold water, the precipitate was dissolved in 10 mM NaOH to 2.5–3.5 mg/ml. The purity of the B chain was confirmed to be > 95 % by the ^{1}H signals of ε protons in tyrosine residues obtained using the NMR spectrometer. The purified insulin B chain was stored at -80 °C before use.

The stock insulin B chain in 10 mM NaOH was diluted with 50 mM Tris-HCl buffer at a concentration of 1.4 mg/ml, which was then put in a 1-mm path-length quartz cell. The small angle X-ray scattering (SAXS) pattern was collected at 25 °C with NANOPIX equipped with HyPix-6000 (Rigaku Corporation, Japan). A Cu K-α line (MicroMAX-007HF) was used as a beam source, which was further focused and collimated with a confocal multilayer mirror (OptiSAXS). The camera length was set to 1.33 m and the range of the scattering vector q was from 0.006 to 2.35 Å^{-1}. Scattering data were collected with an exposure time of 30 min at an interval of 30 min.

RESULTS: Fig. 1 shows representative SAXS profiles of insulin B chain monitored in the formation process of the prefibrillar intermediates. Significant changes in these scattering profiles indicated that the SAXS profiles successfully tracked the formation process of the prefibrillar intermediates. Interestingly, the slope of the log-log plot of the scattering profile was close to −1 from the beginning, suggesting that insulin B chain aggregates in a rod-like shape.

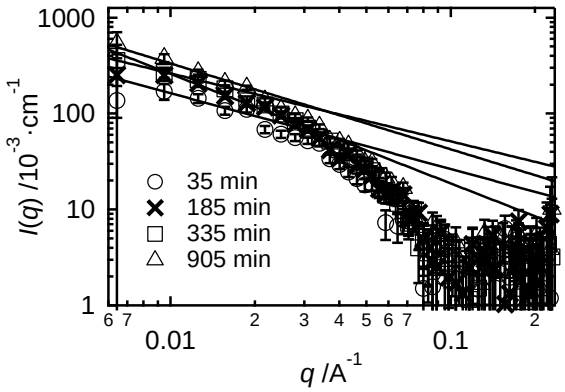

Fig. 1. Representative one-dimensional SAXS profiles of insulin B chain monitored at 35, 185, 335, and 905 minutes. The lines indicate slopes obtained by curve fit.

Data analysis is now ongoing to investigate details about time evolution of conformational development from monomers towards the prefibrillar intermediates. A preliminary analysis of the cross-section plot suggested that the base radius (R_c) of the rod-like aggregates gradually increased from 20 to 25 Å during the measurement. Furthermore, dynamic light scattering measurement allowed us to obtain the hydrodynamic radius, R_h. With the R_c and R_h values, we are now attempting to estimate the length of the prefibrillar intermediate based on Broersma's relationship. The accomplishment of the analysis will reveal detailed mechanisms of the formation of the prefibrillar intermediates of insulin B chain.

REFERENCES:

[1] E. Chatani and N. Yamamoto, Biophys. Rev., **10** (2018) 527-534.
[2] N. Yamamoto *et al*., Sci. Rep., **8** (2018) 62.
[3] E. Chatani and R. Inoue *et al.,* Sci. Rep., **5** (2015) 15485.
[4] A.E. Langkilde and B. Vestergaard, FEBS Lett. **583** (2009) 2600-2609.

CO6-8 Analysis of the initial step of fibrillation by amyloid-β peptide

T. Nakagawa, D. Tsuri, I. Nishii[1], K. Morishima[2], R. Inoue[2], M. Sugiyama[2] and M. Hoshino

Graduate School of Pharmaceutical Sciences, Kyoto University
[1]Faculty of Science, Nara Women's University
[2]KURNS, Kyoto University

INTRODUCTION: Alzheimer's disease is a progressive neurodegenerative disorder. One of its pathological hallmarks is the extracellular deposition of senile plaques in the brain. The major component of these plaques is fibrillar aggregates (amyloid fibrils) of amyloid β-peptide (Aβ). Although the conversion of soluble Aβ monomers to insoluble amyloid fibrils is considered to be a key step to understand the development of Alzheimer's disease, little is known about the molecular mechanism of this process.

The difficulty to analyze the initial step of fibril formation is mainly originated from the extraordinarily high cooperativity of the reaction. While the solution of monomer peptides seems quiescent before the formation of the "nucleus" of amyloid fibrils, a numerous number of molecules rapidly and almost irreversibly bind to the "nucleus" once it formed. As a result, the most important intermediate, "nucleus" or "soluble oligomer", exists only rarely and temporarily.

Here, we examine the conformation of a covalently linked Aβ dimer peptide as a model compound for the initial intermediate of the amyloid fibril formation. We found that the aggregation reaction was enhanced remarkably by the covalent link of two molecules. However, the conformation of tethered molecule was, by itself, very similar to that of random coil structure. We also found that morphology of the aggregates depended significantly on the peptide concentrations. From these observations, we propose that formation of amyloid fibrils are governed by a delicate balance between association and dissociation rate constants.

EXPERIMENTS: The wild type and mutant Aβ(1–40) peptides were constructed as fusion proteins with ubiquitin. The proteins were expressed and purified as described previously [1].

Transmission electron microscopy observations were performed on a JEOL JEM JEM-2100F electron microscope with an acceleration voltage of 100 kV. Samples were applied to Formvar-coated grids and negatively stained with 2% (w/v) uranyl acetate.

NMR experiments were performed on a Bruker Avance 600 spectrometer with triple-resonance probe. A typical ^{1}H-^{15}N HSQC experiments were performed at protein concentration of 50 μM. The solvent conditions used were 20 mM sodium acetate (pH 5.0), and 10% D_2O. The chemical shift value was referenced to DSS.

The kinetics of the aggregation of Aβ peptides was monitored as the increase in fluorescence of thioflavin T (ThT) measured at 490 nm with an excitation wavelength of 446 nm on a Shimadzu RF-5300 spectrofluorometer.

RESULTS: In order to prepare a covalently linked-dimer Aβ peptide, we introduced a cysteine residue by substituting alanine residue at the second N-terminal position. By oxidizing two ceysteine residues, Aβ molecules were covalently linked in the parallel orientation, which was called as A2C-dimer. In contrast to the wild type Aβ peptide, in which fibril formation is preceded by a long lag-period (typically 12~24 hrs), incubation of A2C-dimer resulted in a rapid increase in ThT fluorescence. Dynamic light scattering experiments also suggested rapid formation of aggregates with hydrodynamic radius of several hundred nm. A detailed analysis by TEM observation revealed, however, the morphology of rapidly formed aggregates by A2C-dimers was different from those by wild type Aβ.

Next, we attempted to examine the conformation of A2C-dimer peptide by high resolution NMR spectroscopy in detail. Because rapid formation of aggregate by A2C-dimer hampered analysis by solution NMR, we encapsulated a molecule of A2C-dimer into a reverse micelle formed by mixture of Aerosol-OT(AOT) and hexane to prevent spontaneous aggregation. Surprisingly, the NMR spectrum of A2C-dimer isolated in AOT micelle was almost identical to that of wild type Aβ molecule, suggesting that both Aβ species assume a random coil like structure (Fig. 1).

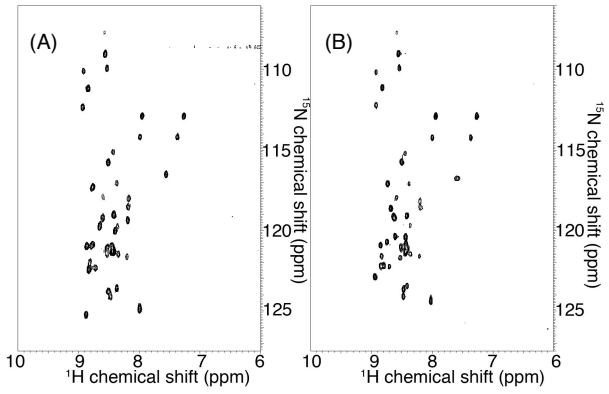

Fig. 1. ^{1}H-^{15}N HSQC spectra of wild type Aβ peptide in aqueous solution (A) and A2C-dimer in AOT/hexane reverse micelle (B).

The results of NMR analysis suggested that the molecular structure of Aβ peptides was, by itself, not significantly changed. Instead, the difference in the kinetics of aggregate formation as well as the morphology of them might attribute too strong tendency of aggregate formation in A2C-dimer peptide. The results emphasizes the importance of delicate balance of the association and dissociation rate constants for the formation of "one-dimensional crystal", amyloid fibrils.

REFERENCES:

[1] T. Yamaguchi *et al*., Biochemistry (2010) 49, 7100-7107.

CO6-9 Generation of radioresistant *Escherichia coli* by adaptive evolution using gamma rays as selection pressure

T. Saito

Institute for Integrated Radiation and Nuclear Science, Kyoto University

INTRODUCTION: In nature, organisms have evolved diversely by adapting themselves to various environmental conditions. Some organisms have been found to survive in environments that can be easily perceived as extremely severe. Elucidating the adaptive mechanisms of organisms to severe environmental conditions can provide meaningful information regarding evolution and diversity overall. Some bacteria, known as radioresistant bacteria, demonstrate extreme resistance to ionizing radiations. The extreme resistance mechanism of these bacteria to ionizing radiation is an interesting area of research from the standpoint of adaptive mechanisms employed by organisms in nature. In order to elucidate the mechanisms of radioresistance in these organisms, it is important to investigate their biological defense mechanisms against external stresses at the molecular level. However, studies conducted on radioresistant organisms existing in nature are likely to encounter many challenges due to limited knowledge of their genetic and biochemical properties. Therefore, in this study, the generation of radioresistant cells of *Escherichia coli* was attempted by experimenting on their ability to undergo adaptive evolution when exposed to gamma rays The following operations were repeated in this experiment: gamma-ray irradiation of *E. coli* cells whose genetic and biochemical properties are sufficiently known, growth of the surviving cells, and irradiation of the grown cells.

EXPERIMENTS: Evaluation of the sensitivity of *E. coli* cells to gamma irradiation: *E. coli K*-12 cells were grown to the early log phase in LB medium at 37°C at 200 rpm. One milliliter of the culture was centrifuged at 4000 × *g* at 20°C for 10 min. The supernatant was discarded and the pellet was suspended in 1 mL of PBS (–). The cell suspension was irradiated with gamma rays at a dose rate of 22 Gy/min at 20 ± 3°C. Gamma irradiation was carried out at the Co-60 Gamma-ray Irradiation Facility of the Institute for Integrated Radiation and Nuclear Science, Kyoto University. The gamma-irradiated cell suspension was diluted appropriately with PBS (–), plated on LB agar, and incubated at 37°C for 12 hr. After incubation, the colonies were counted, colony forming units were determined, and survival rates were calculated.

Selection with gamma rays: *E. coli K*-12 clone cells obtained by single colony pick-up were cultured to the early log phase in LB medium at 37°C at 200 rpm. The cell suspension was prepared as described above and irradiated with the 1% survival dose of gamma rays at a dose rate of 22 Gy/min at 20 ± 3°C. One milliliter of the gamma-irradiated cell suspension was inoculated in 100 mL of LB medium and cultured at 37°C at 200 rpm till the cells reached their early stationary phase. The glycerol stock was prepared and stored at –80°C. This procedure was repeated after culturing the glycerol stock cells to the early log phase.

RESULTS: In order to generate radioresistant *E. coli* cells by adaptive evolution to gamma rays as the selection pressure, *E. coli* cells were irradiated with a 1% survival dose of gamma rays, and the surviving cells were grown. The 1% survival dose of the surviving cell population to gamma rays was evaluated, and the cell population was once again irradiated with the 1% survival dose. The 1% survival dose to gamma rays of the wild type *E. coli* clone without selection was 242 Gy, whereas that of the *E. coli* population obtained after 20 selection cycles was 1872 Gy; the resistance of *E. coli* to gamma rays was increased 7.7 fold in this adaptive evolution experiment (Fig. 1). Furthermore, the resistance gradually increased in the process of the adaptive evolution. These results indicate that mutations and changes in the expression levels of many genes are likely to be involved in this increase of resistance. In the future, further studies, namely that the gene expression levels of radioresistant *E. coli* cells obtained by the adaptive evolution experiment are analyzed and compared with those of wild type *E. coli* cells, will be required.

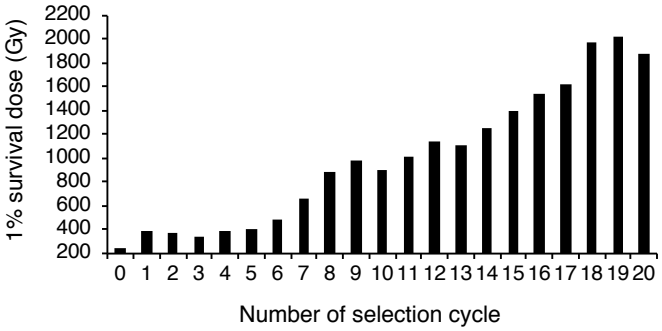

Fig. 1. Increase in resistance of *E coli* cell populations to gamma rays during adaptive evolution.

REFERENCES:

[1] T. Saito, Viva Origino, **30** (2007) 85–92.

CO6-10 Physicochemical study on ILEI suppressing amyloid-β generation

E. Hibino[1], K. Morishima[2], R Inoue[2], M Sugiyama[2], M Nakano[1], N Watanabe[1], T Sugi[1] and M Nishimura[1]

[1]*Molecular Neuroscience Research Center, Shiga University of Medical Science*

[2]*KURNS, Kyoto University*

INTRODUCTION:

The number of patients with Alzheimer's disease (AD) is increasing in Japan. However, any effective AD modifying drug is still undeveloped. The pathogenic processes of AD are thought to be triggered by accumulation of amyloid-β protein (Aβ) in brain. Previously, we have identified a secretory protein named interleukin-like epithelial-mesenchymal transition inducer (ILEI, also known as FAM3 superfamily member C) as a negative regulator of Aβ production by the unique activity[1]. ILEI is secreted from cell to bind to the extracellular region of Presenilin-1, a component of the γ-secretase complex.

The interaction of ILEI with Presenilin-1 enhances nonspecific degradation of Aβ precursor protein. However, the molecular mechanism based on the structural findings is still to be clarified. Although the monomeric and dimeric forms of ILEI have been reported recently[2], the structure-function relationships are also still unclear.

The objective of this study is to elucidate whether the dimerization of ILEI is indispensable for the function on Aβ generation.

EXPERIMENTS:

Human ILEI (residues 55-227) tagged with His was over-expressed in Rosetta-gamiB (DE3) pLysS stain and purified using Ni-NTA resin and size exclusion chromatography (SEC). CBB-stained SDS-PAGE gels and SEC profile on non-redox condition showed a single band and peak, respectively. Subsequently, around 1.5 mg/mL ILEI protein solution was diluted with buffer at each pH condition (6.0, 7.3 and 8.0).

To confirm the monomer-dimer transition of ILEI at 25˚C, ILEI solution was analyzed by analytical ultracentrifugation at 60,000 r.p.m. or 20,000 r.p.m.

RESULTS:

The profiles measured at 60,000 r.p.m. of the rotating speed by Rayleigh interferometer are shown in Fig. 1. The peak derived from around 40 kDa was identified although the main peak corresponding to 20 kDa accounted for the greater part. Most ILEI molecules existed as monomeric state since the molecular weight of ILEI monomer was predicted to be 20.0 kDa. In addition, the abundance ratios of multimer, which were 4.5%, 3.7% and 15.2% at pH 6.0, pH 7.3 and pH 8.0, respectively, were increased in correlation with an increase in pH value.

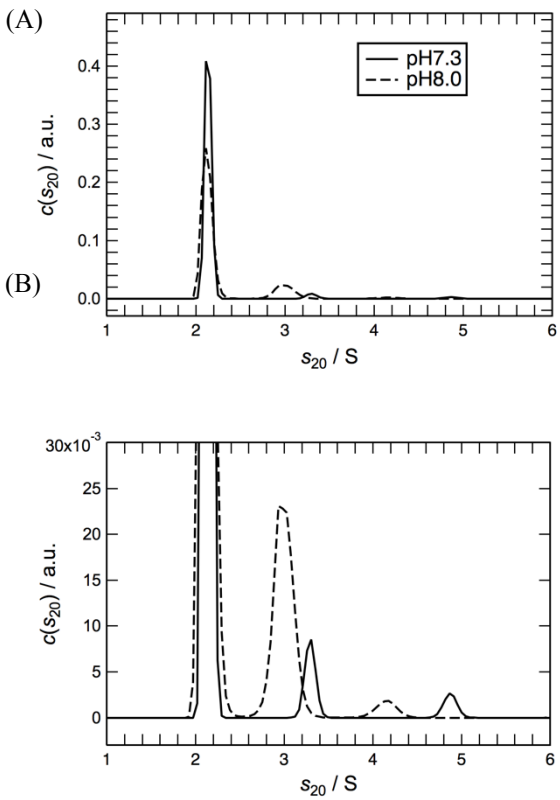

Fig. 1. (A) The solid line, dashed line and dotted line show distributions of sedimentation coefficient derived from ILEI at pH 6.0, pH 7.3 and pH 8.0, respectively. (B) The expanded of the lower range of A.

Furthermore, to identify whether ILEI proteins were dissociated or not, we also measured the profiles at 20,000 r.p.m, so that, the peaks were put into one peak (data not shown). This suggested that ILEI was in monomer-multimer equilibrium state. Moreover, the dissociation constants calculated from the populations were 4.3×10^{-4} M (25℃, pH 7.3) and 1.0×10^{-4} M (25℃, pH 8.0).

In conclusion, although ILEI can form homodimers, most ILEI molecules are thought not to dimerize, taking it consideration that population of dimer is low at pH 7.3 and that ILEI is a secretory protein. We speculate that ILEI functions in monomeric state, although a possibility that ILEI dimers have functions dissimilar from the monomer cannot be ruled out.

REFERENCES:

[1] H. Hasegawa *et al*., *Nat. Commun.*, 5:3917 (2014).
[2] A.M. Jansson *et al*., *J. Biol. Chem.*, **297** (2017) 15501-15511.

CO6-11 **Structural characterization of the *S. pombe* nucleosome containing histone variant H2A.Z**

M. Koyama[1], R. Inoue[2], K. Morishima[2], W. Nagakura[3], M. Sugiyama[2], H. Kurumizaka[1,3]

[1] *Institute for Quantitative Biosciences, The University of Tokyo*

[2] *KURNS, Kyoto University*

[3] *Division of Advanced Science and Engineering, Waseda University*

INTRODUCTION:

In the eukaryotic cells, genomic DNA binds histone proteins to form the chromatin structure, and stored in the nucleus. The structural unit of the chromatin is the nucleosome, in which about 145-base-pairs of DNA are wrapped around the histone octamer, containing two molecules of each of four core histones (H2A, H2B, H3, and H4) [1, 2].

The fission yeast *S. pombe* is a single cell eukaryote that shares many characteristics of the chromatin structure and function with higher eukaryotes. *S. pombe* has only one H2A variant, H2A.Z, which is preferentially associated with actively transcribed chromatin. In this study, to analyze the structural property of the *S. pombe* H2A.Z nucleosome, we reconstituted the nucleosome *in vitro*, and measured its small angle X-ray scattering profile.

EXPERIMENTS:

The *S. pombe* canonical (H2A) or H2A.Z nucleosomes were reconstituted *in vitro*, by mixing a 146-base-pair DNA fragment with *S. pombe* four core histones (SpH2A or SpH2A.Z, SpH2B, SpH3, and SpH4). The reconstituted nucleosomes were further purified by polyacrylamide gel electrophoresis using the Prep Cell apparatus (BioRad). The purified samples were concentrated using a Millipore concentrator (Mw cutoff of 30,000). After filtration, the samples were used for the SAXS measurement.

RESULTS:

SAXS profiles of the *S. pombe* canonical nucleosome, and the *S. pombe* H2A.Z nucleosome are shown in Fig. 1. Guinier plots of the data are shown in Fig. 2. The straight line represents the least-square fitting for the data. This result revealed that the gyration radius (R_g) of the *S. pombe* H2A.Z nucleosome is 46.2 ± 0.3 Å, which is larger than that of the *S. pombe* canonical nucleosome (R_g = 45.0 ± 0.2 Å). The distance distribution functions of the nucleosomes are shown in Fig. 3. The longest distances, D_{max} values, are 150 Å for the canonical H2A nucleosome, and 157 Å for the H2A.Z nucleosome. These findings suggest that the H2A.Z nucleosome has more stretched structure, as compared to the canonical nucleosome in *S. pombe*.

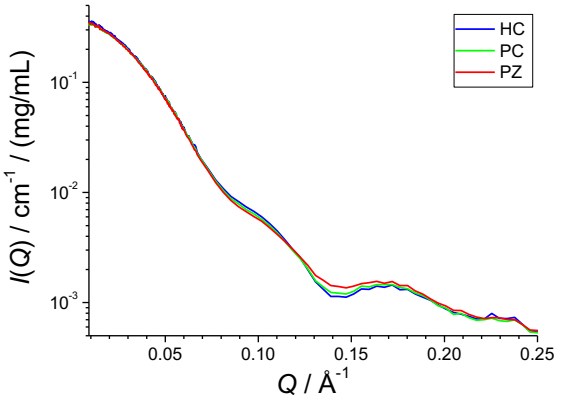

Fig. 1. SAXS profiles of the *S. pombe* canonical nucleosome (green), the *S. pombe* H2A.Z nucleosome (red), and the human canonical nucleosome (blue).

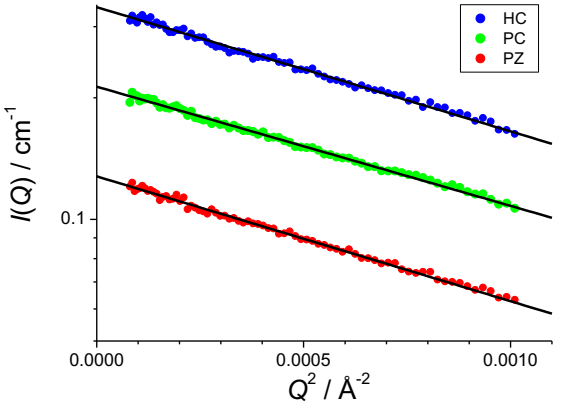

Fig. 2. Guinier plots of the nucleosomes. The color coding is the same as in Fig. 1.

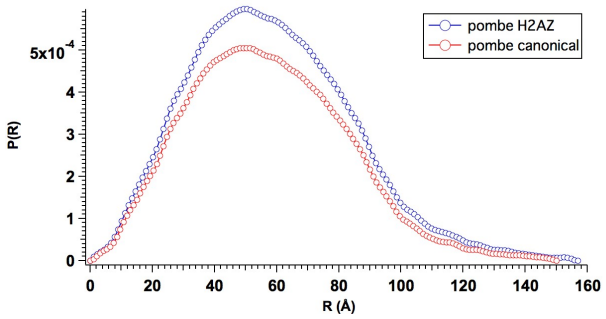

Fig. 3 Distance distribution functions of the *S. pombe* H2A.Z nucleosome (blue) and *S. pombe* canonical nucleosome (red).

REFERENCES:

[1] K. Luger *et al.*, Nature, 389, 251-260 (1997).
[2] M. Koyama and H. Kurumizaka, J. Biochem., 163, 85-95 (2018).

30041

CO6-12 Production of medical radioisotopes using electron linear accelerator

S. Sekimoto, T. Ohtsuki

Institute for Integrated Radiation and Nuclear Science, Kyoto University

INTRODUCTION: A shortage in the supply of ^{99}Mo resulting from the shutdown of reactors used for its production is a global problem. Because ^{99}Mo is an indispensable source of ^{99m}Tc, which is used in nuclear medicine to make diagnoses using techniques such as scintigraphy and single photon emission computed tomography (SPECT), a stable supply of ^{99}Mo is vital. Therefore, production of ^{99}Mo by using neutrons or protons generated in accelerators has been investigated [1–3]. To separate ^{99m}Tc from ^{99}Mo produced by an accelerator, methods based on sublimation, solvent extraction, and ion-exchange column chromatography have been examined and developed [2,4–6]. In addition, Gopalakrishna et al. have reported the preparation of ^{99}Mo by the ^{100}Mo(γ,n) reaction using bremsstrahlung photons [6], followed by conventional solvent extraction using methyl ethyl ketone (MEK) and zirconium (Zr) molybdate gel to separate ^{99m}Tc. According to the regulations of the Japanese pharmacopeia, the extraction using organic materials and the gel method using heavy metal elements such as Zr are not approved for the ^{99m}Tc-separation methods. Additionally, it is also difficult and impractical to use the sublimation method, which requires complicated and/or large scale devices for the mass-production of pure ^{99m}Tc.

In the previous work, we carried out the production of ^{99}Mo by the ^{100}Mo(γ,n) reaction using bremsstrahlung photons generated in an electron linear accelerator (LINAC), a technique that has not been investigated significantly in Japan. The amounts of ^{99}Mo produced at several electron energies (E_e) were examined. In this report, the amounts are compared with those predicted by calculation. The experimental condition and results are described in ref. [7].

RESULTS: The ^{99}Mo activities in the pellets were calculated by using the particles and heavy ion transport code system (PHITS) [8], and the calculated values are shown in Fig. 1 for comparison with the experimental values. Although the experimental value at an E_e of 32 MeV agrees with the calculated value, the experimental values are lower than those calculated at E_e's of 21 and 25.5 MeV and higher than those calculated at E_e's of 35 and 41 MeV. These differences between experimental and calculated values can be explained by the dispersion of the photon beams. At higher E_e, in general, the intensity of electrons in the longitudal direction is greater than that of electrons in the transverse direction; *i.e.*, the dispersion of higher energy electron beams (higher E_e) tends to be smaller than those at lower E_e due to the space charge density of electrons. Therefore, the dispersion of photon beams generated by electrons at higher E_e becomes smaller. This tendency can be confirmed by simulation using the Geometry and Tracking (GEANT) code. Because the dispersion of the photon beams in the PHITS calculation performed in this work is assumed to be identical at E_e's between 21 and 41 MeV, a disagreement was found between the experimental and calculated values. However, the validity of the experimental ^{99}Mo is supported by those found for ^{196}Au produced via the ^{197}Au(γ,n) reaction, *e.g.*, the E_e dependence of the rate of ^{99}Mo-production is similar to that of ^{196}Au-production. This trend depends on the fact that the shape of the excitation functions for the photon energies in the ^{100}Mo(γ,n) and the ^{197}Au(γ,n) reactions are similar, although the absolute values are different by about one order of magnitude [9].

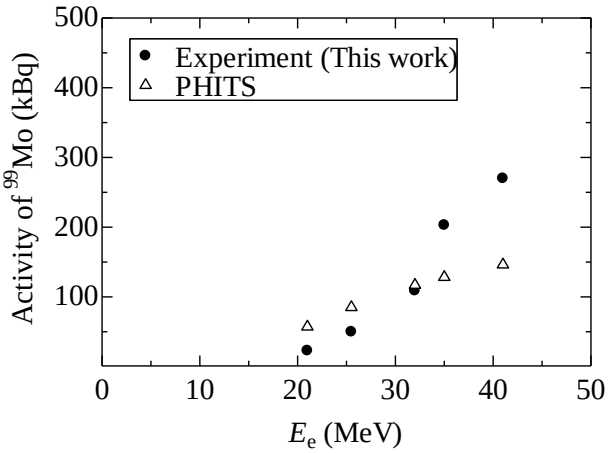

Fig. 1. Activity of ^{99}Mo produced using electron linear accelerator (The irradiation time, beam current of electrons, and amount of target material ($^{100}MoO_3$) were normalized to 5 min, 100 micro-A, and 10 mg, respectively.)

REFERENCES:

[1] Y. Nagai *et al.,* J. Phys. Soc. Jpn. , **82** (2013) 064201.
[2] Y. Nagai *et al.,* J. Phys. Soc. Jpn. , **83** (2014) 083201.
[3] K. Nakai *et al.,* Proc. Jpn. Acad. Ser. **B 90** (2014) 413–421.
[4] M. Kawabata *et al.,* J. Phys. Soc. Jpn. , **84** (2015) 023201.
[5] K. Mang'era *et al.,* J. Radioanal. Nucl. Chem., **305** (2015) 79-85.
[6] A. Gopalakrishna *et al.,* J. Radioanal. Nucl. Chem., **308** (2016) 431-438.
[7] S. Sekimoto and T. Ohtsuki, KUR-progress report (2017) CO6-14.
[8] Niita K *et al.,* (2010) PHITS: Version 2.23, JAEA-Data/Code 2010-022, JAEA.
[9] Dietrich SS, Berman BL (1988) Atlas of photoneutron cross sections obtained with monoenergetic photons. Atomic Data Nucl Data Tables. 38:199–338.

CO6-13 Determination of degree of deutteartion level of deuterated protein through small-angle neutron scattering

R. Inoue, K. Morishima, N. Sato, M. Sugiyama

Institute for Integrated Radiation and Nuclear Science, Kyoto University

INTRODUCTION: Small-angle Neutron (SANS) technique gives the overwhelming opportunities for structural analyzes on target samples in solution. Especially, contrast-variation SANS (CV-SANS) method [1], which utilizes the modulation of scattering length density (scattering contrast) between solute and solvent, offers the fascinating opportunity for studying the partial structure of complex biological samples. It is known that the scattering length density of normal (or hydrogenated) protein is nearly equal to that of 40% D_2O. Namely, hydrogenated protein is invisible in 40% D_2O in terms of CV-SANS. With this characteristic feature, the CV-SANS method has been applied for various hydrogenated proteins. On the other hand, on of the big disadvantages associated with above CV-SANS method is high incoherent signal from 60% H_2O, hindering the detailed structural analyzes on target biological samples. In order to overcome such a situation, the inverse contract matching SANS (ICM-SANS) method [1] has been paid attention. The essence of this technique is that the scattering length density of protein is tuned to be matched with that of 100% D_2O by modulating the deuteration level of protein. The most stressing point in ICM-SANS is the realization of high S/N SANS data attained by the suppression of incoherent scattering from solvent. However, the procedure for preparation of partially deuterated protein that is perfectly contrast-matched with 100% D_2O has not been well established up to now. For this purpose, we have to grasp the proper deuteration condition and the protocol for the determination of degree of deuteration of prepared partially deuterated protein. It is considered that SANS and mass spectrometry are usable for the determination of degree of deuteration of prepared partially deuterated protein. Prior to usage of SANS meausremnets, we try to determine the degree of deuteartion of partially deuterated protein with mass spectrometry.

EXPERIMENTS: In addition to the preparation of hydrogenated αB-crystallin, we prepared partially deuterated αB-crystallin by mixing ratio of hydrogenated and deutearted glucose 3:1 in 75% D_2O. Mass spectrometry measurements were performed with microflex, BRUKER.

RESULTS: Fig. 1 shows mass spectrum from hydrogenated αB-crystallin and partially deuterated αB-crystallin, respectively. It can be clearly seen that main peak shifted to high m/z value by deuteration, implying the exact increase of mass during cultivation.

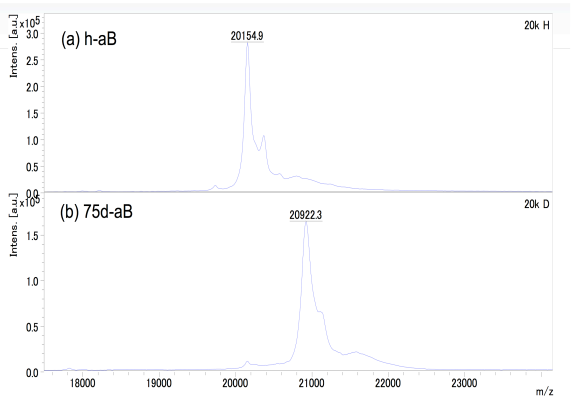

Fig. 1 (a) Mass spectrum from hydrogenated αB-crystallin. (b) Mass spectrum from partially deuterated αB-crystallin.

Considering the amino acid sequence of αB-crystallin, we have calculated the degree of deuteration of partially deuterated αB-crystallin. The degree of deuteartion of partially deuterated αB-crystallin was found to be 70.0%. As written at the experimental section, we have cultivated partially deuterated αB-crystallin in 75% deuterated glucose and 75% D_2O. Hence, the resulting degree of deuteartion of prepared αB-crystallin is much lower than 75%. It is expected that further control of cultivation condition such as mixing ratio of deuterated glucose must be taken into account.

As a next step for this project, we are now trying to evaluate the degree of deuteartion of αB-crystallin by changing the mixing ratio of deuterated glucose and D_2O. It will contribute to realizing the perfectly contrast-matched partially deuterared protein in 100% D_2O. It will further reinforce the powerfulness of ICM-SANS.

REFERENCES:

[1] M. Sugiyama *et al.*, BBA, **1862** (2018) 253-274.

CO6-14 Measurement of Trancemitance Spectra of a Humann Calcificated Aorta Tissue in the Sub-Terahertz Region, which Related with a SEM-EDX Elements Imaging (II)

N. Miyoshi and T. Takahashi[1]

Department of Molecular Chemistry, Kyoto Institute of Technology
[1]Institute for Integrated Radiation and Nuclear Science, Kyoto University

INTRODUCTION: The LINAC (Electron linear accelerator) technology in the millimeter- and terahertz-waves had been unique and had been used as a coherent synchrotron light source in the Institute for Integrated Radiation and Nuclear Science of Kyoto university (KURNS) to observe the transmittance spectra of a human calcified aorta tissue as a collaborate study. The absorption spectra in the sub-terahertz region had been not so clear for the raw tumor tissue although Ashworth-PC. *et al.* [1] had reported for the excised human breast cancer by a terahertz pulsed spectroscopy observed at 320 GHz, which was estimated a longer relaxation time component of the induced electricity for water molecules [2-3] in the raw tumor tissue for three years at the linear analysis.

We had started to measure of new biological sample of a calcified human aorta dried tissue sampling from the pathological autopsy in the last year. Furthermore, the getting spectral information was estimated with the SEM-EDX elements images of the calcified aorta tissue with a biological meaning in this year. It was reported the relation of the biological information between both of the element images and sub-THz spectral components in this report.

EXPERIMENTS: (1) Instrument of Near-field in Terahertz Region: The photograph of the instrument was shown in Fig. 1. Mark-A: Pre-probe Wiston cone; 50-10mm diameter, Length=60mm; the irradiate diameter=0.775mm; Mark-B: The concentrate light probe (diameter=3mm). The instrument was developed by Dr. T. Takahashi [4] for the transmittance measurements.

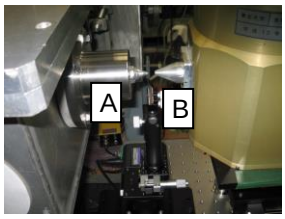

Fig. 1. The near field area of sample holder position.

(2) Sample Preparation for SEM-EDX Elements (P, and Ca) Images of Calcified Aorta: A calcified aorta tissue was cryo-sectioned in vertical of the blood wall at -20 ℃ at 8 μm depth. The sample tissues was measured by a Scanning Electron Microscope (JEOL) combined with Energy Dispersion X-ray (EDX) analyzer.

RESULTS and DISCUTION: (1) The morphological images were observed in side of the calcified aorta tissue by the SEM-EDX analysis as shown inf Fig. 2.

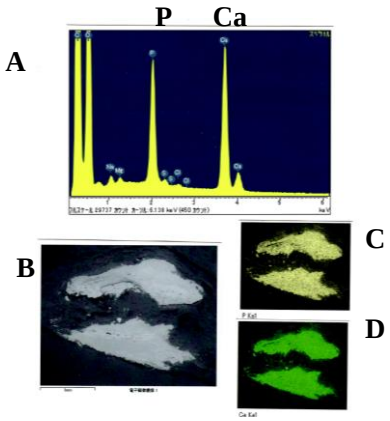

Fig. 2. The SEM-EDX spectrum (A), the SEM, the elements (P and Ca) vertical images (B, C and D) of a human calcified aorta blood vessel wall, respectively.

(2) The transmittance spectra of the sample tissue for each points A, B and C were measured (Fig. 3).

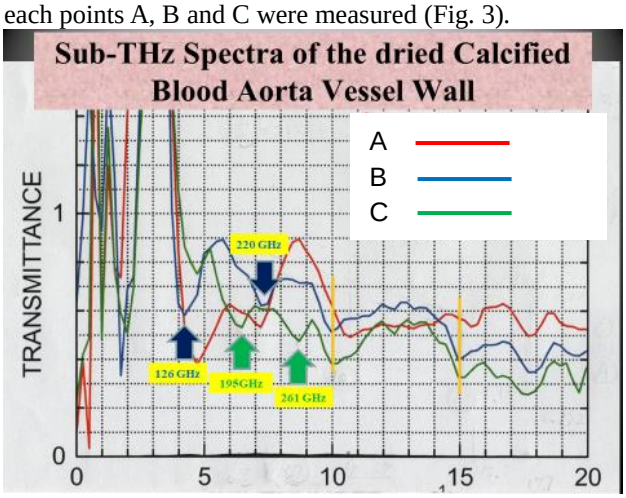

Fig. 3. Sub-THz spectra of the dried calcified blood aorta vessel wall. (A: calcified; B: cholesterol; C: normal)

In the results, the absorbance of the dried tissue at 195 and 261 GHz were observed in the calcified area (included of $CaPO_4$ components from the data of SEM-EDX analysis of calcified aorta tissue), and the absorption peaks of 125, 220 GHz were observed in the cholesterol adhesion area. In the both areas, it was observed the absorption peaks at 300 and 450 GHz also.

In future, it will be needed more measurements and analysis combined with the depth information data of the dried tissue by an ultrasound measurement technology.

REFERENCES:

[1] Phillip C. Ashuworth *et al.*, Optics Express, **17** (2009) 12444-12454.
[2] Toshiko Fukasawa, *et al.*, Phys. Rev. Lett., **95** (2005) 197802.
[3] Hiroyuki Yada, *et al.*, Chem. Phys. Lett., **464** (2007) 166-170.
[4] T. Takahashi, *et al.*, J. Phys.: Conf. Ser. **359** (2012) 012016-1-4.

CO6-15 Preparation of bovine intact FoF1ATP synthase for a cryo-EM structural analysis

C. Jiko[1], C. Gerle[2] and Y. Morimoto[1]

[1]*Institute for Integrated Radiation and Nuclear Science, Kyoto University*
[2]*Institute for Protein Research, Osaka University*

INTRODUCTION: Atomic resolution structure analysis of biomolecules using cryo-electron microscopy (cryo-EM) has been developed (Henderson et al., Nobel Prize, 2017) and the analysis is currently overwhelming for study of membrane proteins that are extremely difficult to crystallize. Although it is powerful, the key to success in structural analysis by a cryo-EM is the ability to purify large quantities of stable and intact samples as well as crystallization.

In this study, we aim to analyze the full length of mammalian mitochondrial FoF1 ATP synthase with atomic resolution. An FoF1 ATP synthesis is an important energy conversion mechanism for maintaining mammalian life activities, and is driven by proton transport in the mitochondrial inner membrane. The FoF1 ATP synthase responsible for this is a membrane protein complex with a molecular weight of 600,000 consisting of 29 subunits. The enzyme not only produces 90% of ATP but also plays an important role in the formation of the inner mitochondrial membrane. It is also suggested that dysfunction of this enzyme leads to apoptosis (cell death). Threfore elucidation of the precise three-dimensional structure of this enzyme is considered to be an important basis for drug molecule design in the future, and is widely studied.

Because of this biological and medical importance, efforts to elucidate the structure of the FoF1 ATP synthase have been made for over 50 years, but the understanding of the function of the FoF1 ATP synthesis enzyme is delayed by the fact that the entire structure has not been elucidated at the atomic level.

The enzyme is a membrane-bound protein of the macromolecule complex and is highly flexible and unstable because of its rotation, which makes it difficult to obtain a purified preparation having a uniform three-dimensional structure throughout the enzyme.

EXPERIMENTS: Bovine heart was obtained immediately after slaughter, and mitochondrial inner membrane was separated followed by solubilization of FoF1 ATP synthase. At this time, purification was required in order to solubilize other proteins. As a purification method of this enzyme, one using an affinity column such as ion exchange chromatography is generally used, and we have also purified by the same method.

However, it was found that this method led to low uniformity of the purified sample. This is because the enzyme has extremely high flexibility as it rotates, and the subunit of this enzyme, which is composed of as many as 29 subunits per monomer, starts dissociation from the intermembrane domain during the purification process

Although this ion exchange chromatography is effective for improving the purification purity, it is considered that the interaction with the ion exchange resin places a burden on the original structure of the enzyme and the degradation of this enzyme is caused. Therefore, it is necessary to establish a purification method that can replace ion exchange chromatography. Dealing with this issue, we developed a purification method by density gradient centrifugation without loading the protein (column-free purification) and succeeded in purifying the enzyme in a very stable and intact state.

RESULTS and DISCUSSION: Using this stable enzyme with full subunits, prepared by the column-free purification developed by the applicant, it was possible to produce a cryogrid suitable for high-resolution single particle analysis by cryo-EM (Fig. 1).

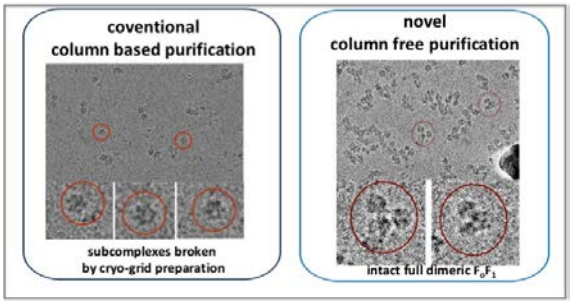

Fig.1 Recent images of mammalian FoF1 dimers by cryo-electron microscopy.

Although the greatest obstacle to collecting high quality data of membrane proteins is the detergent (Rubinstein, Methods, 2007), usually, when the detergent is removed from solution, membrane proteins aggregate and denatures instantaneously. On the other hand, the method developed by Gerle et al. (GraDeR; Hauer et al., Structure, 2015) makes it possible to remove the detergent in the solution before the instant freezing of grid preparation. Currently, grid adjustment is carried out using this method, and observation by cryo-EM is being conducted.

ACKNOWLEDGEMENT: This work is partly supported by the grant of Naito foundation 2018, the grant-in-aid for the young researchers of the JSPS 2019 (C.J.) and the TERUMO foundation 2018, the grant for an advanced research of the KURRI 2018 (Y.M.) .

CO6-16 Preclinical study of boron neutron capture therapy for bone metastasis using human lung cancer cell lines

T. Andoh[1], T. Fujimoto[2], Y. Nagasaki[1], M. Suzuki[3], H. Tanaka[4], T. Takata[4], Y. Sakurai[4], and H. Ichikawa[1].

[1]*Faculty of Pharmaceutical Sciences, Kobe Gakuin University, Japan.*
[2]*Department of Orthopaedic Surgery, Hyogo Cancer Center, Japan.*
[3]*Particle Radiation Oncology Research Center, Institute for Integrated Radiation and Nuclear Science, Kyoto University, Japan.*
[4]*Division of Radiation Life Science, Institute for Integrated Radiation and Nuclear Science, Kyoto University, Japan*

INTRODUCTION: Lung cancer is the leading cause of cancer-related death globally [1]. Rapid metastasis to the bone can occur in 25-40% of lung cancer patients, which has a poorer prognosis [2]. When systematic pharmacotherapy is not effective, the disease is difficult to control. Boron neutron capture therapy (BNCT) may be the sole option in such cases. We have previously demonstrated the effectiveness of BNCT with the use of *p*-borono-L-phenyl-alanine (L-BPA) on tumors in the limbs of human clear cell sarcoma-bearing nude mouse models [3]. In the present study, we established a bone metastasis model for lung cancer and investigated *in vivo* biodistribution of L-BPA and antitumor effects after BNCT in the bone metastasis model.

EXPERIMENTS: Cells of A549-luc, a lung cancer cell line of human origin, were suspended in Matrigel® and injected into the tibia of the left hind leg of nude mice [4]. After 3-4 weeks, a tumor mass was observed in tibia of the mice using a computed tomography scan and luminescence imaging. The biodistribution of ^{10}B was explored by the intravenous administration of BPA-fructose complex (BPA-Fr, 24 mg ^{10}B/kg) to a bone metastasis mouse model of lung cancer. At a predetermined time after administration, the mice were sacrificed and blood and tissue samples were immediately collected. The concentration of ^{10}B in the samples was then measured by inductively coupled plasma atomic emission spectroscopy. In the BNCT trial, the model mice were allocated into a BNCT and control groups. The tumors in the left hind legs were exposed to thermal neutron irradiation at the Institute for Integrated Radiation and Nuclear Science, Kyoto University.

RESULTS: Bone metastasis was successfully produced in the human lung cancer-bearing mouse model. The formation of a solid tumor mass in the left tibia of mice was confirmed by macroscopic observation, micro-computed tomography scans, and luminescence imaging. At 1.5 h after the administration of BPA-Fr, the concentration of ^{10}B in the bone metastasis model tumor tissue reached 50 μg ^{10}B/g wet tumor tissue. Tumor-to-blood and tumor-to-normal tissue (normal bone) ratios were 6.3 and 5.7, respectively, at 1.5 h after injection. In the BNCT trial, tumor growth was observed in the control group, while the BNCT group displayed suppressed tumor growth (Fig. 1). These results suggested that ^{10}B accumulates specifically in the bone tumor and that BNCT destroys tumor cells only at the site of lung metastasis.

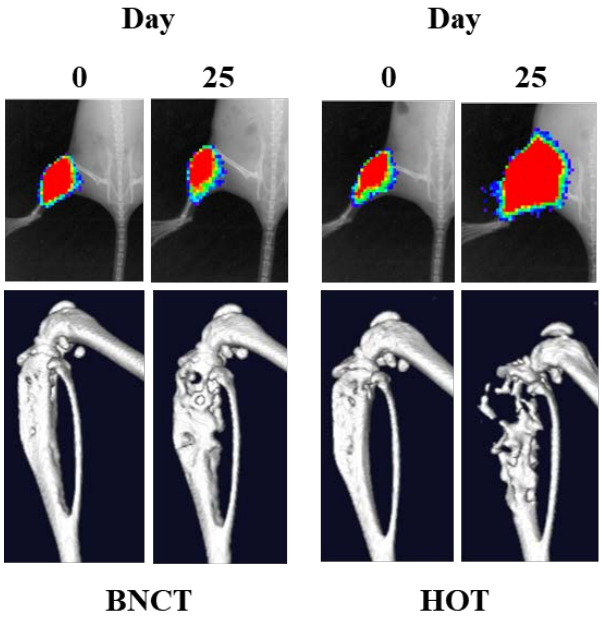

Fig. 1. IVIS images and X-ray CT images after thermal neutron beam irradiation of BNCT and HOT control groups.

REFERENCES:

[1] H.K. Weir *et al.*, J Natl Cancer Inst, 95, 1276–1299 (2003).
[2] H. Fujita, *et al*., PLOS ONE. 11(10) e0164830. DOI:10.1371/journal.pone.0164830 (2016).
[3] T. Fujimoto *et al*. Appl. Radiat. Isot. 73, 96-100 (2013).
[4] J.P. Campbell *et al.*, J. Vis. Exp., 4(67), e4260 (2012).

CO6-17 Coherent Transition Radiation mm-Wave Light Source with an Electron Linac for Absorption Spectroscopy and Irradiation

S. Okuda[1], Y. Tanaka[1] and T. Takahashi[2]

[1]*Organization for Research Promotion, Osaka Prefecture University, Sakai, Osaka, Japan*

[2]*Institute for Integrated Radiation and Nuclear Science, Kyoto University, Kumatori, Osaka, Japan*

***Abstract*—The coherent transition radiation from bunched electron beams of a linear accelerator has continuous spectra in a sub-mm to mm range and has extremely high peak intensity. In Kyoto University the coherent transition light source was developed by using a 45 MeV electron linear accelerator. In this work the characteristics of the light source have been measured and the system has been modified for the applications to absorption spectroscopy and irradiation.**

I. INTRODUCTION

THE coherent transition radiation (CTR) from high-energy bunched electron beams of a linear accelerator (linac) has continuous spectra in a sub-mm to mm wavelength range. The CTR light source has been established [1, 2] by using the electron beams of the 45 MeV L-band electron linac in Kyoto University. It has extremely high peak-intensities in a picosecond light pulse compared with the other THz light sources. The light source has been applied to absorption spectroscopy for various kind of matters. In the present work the detailed properties of the light source have been measured. The light source system has been changed for the applications to absorption spectroscopy and irradiation to investigate the nonlinear effects or biological effects.

II. EXPERIMENTAL

The configurations of the light source system changed for the absorption spectroscopy and the irradiation with CTR are schematically shown in Fig. 1. The electron linac in Kyoto University was used in the experiments. In most experiments the beam energy, macropulse length and the repetition rate are 42 MeV, 47 ns and 60 Hz, respectively. The output CTR light from a light source chamber was transported out from the accelerator room. The spectrum of the CTR light was measured with a Martin-Puplett type interferometer and a liquid-He-cooled silicon bolometer. In the absorption spectroscopy the sample was located on the light path between the interferometer and the detector. The wavenumber resolution was 0.1 cm^{-1} in most experiments, which can be changed. In the interferometer the incident light is divided into two parts by a polarizer: one for spectroscopy and another for irradiation experiments.

III. RESULTS

The light source spectrum has a peak at a wavenumber of about 7 cm^{-1}. The wavenumber range used for spectroscopy was evaluated to be 2-35 cm^{-1}, in which the highest number is limited by the sensitivity of the detector. The intensity of light was estimated to be about 10^{-7} W/0.1%b.w. about the spectral peak and was found to be sufficiently high even if it reduces by 6 orders from the initial one after transmission through the sample with relatively strong absorption. The pulse structure of the CTR corresponds to that of the electron beam from the linac. The micropulse length of the CTR was evaluated by the interferogram obtained by the interferometer to be about 3 ps. Such a relatively short pulse length is due to the special bunching process in the optimized operational conditions of the linac. These results indicated that the peak light intensity in the micropulse is about $3x10^6$ W. In order to increase the peak intensity the electron-gun pulser has been developed to generate the single-bunch electron beam. By using this system it is expected to be a few tens of MW. While the averaged CTR power is sufficiently low not to induce thermal effects in the samples, the comparatively high peak power might cause any nonlinear effects.

Some results for the absorption spectroscopy for liquid samples and the irradiation to investigate the biological effects especially on the gene of fruit fly, *Drosophila melanogaster*, are ongoing to be analyzed.

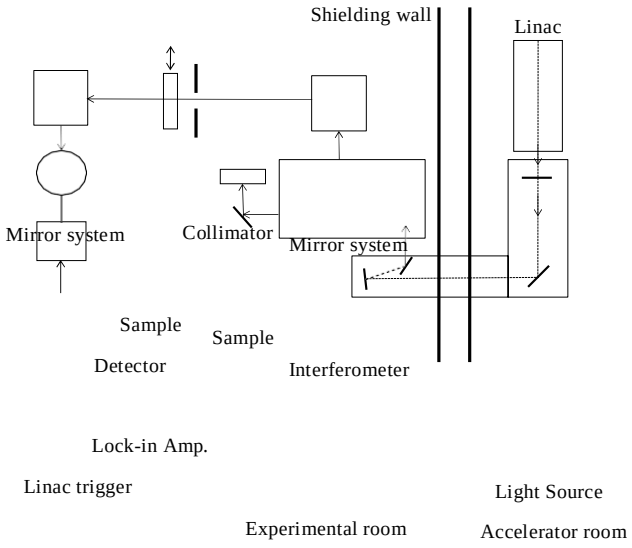

Fig. 1. Schematic diagram showing the configurations for absorption spectroscopy and irradiation using CTR.

In conclusion, the characteristics of the CTR light source in Kyoto University have been measured and the system has been changed for absorption spectroscopy and irradiation experiments. The light source will be applied to investigating some nonlinear effects and biological effects.

This work has been carried out in part under the Visiting Researcher's Program of the Research Reactor Institute, Kyoto University, and supported by JSPS KAKENHI Grant Number JP15K04733.

REFERENCES

[1]. T. Takahashi, T. Matsuyama, K. Kobayashi, Y. Fujita, Y. Shibata, K. Ishi and M. Ikezawa, "Utilization of coherent transition radiation from a linear accelerator as a source of millimeter-wave spectroscopy", *Review of Scientific Instruments*, vol. 69, pp. 3770-3775, 1998.

[2]. S. Okuda and T. Takahashi, "Absorption spectroscopy using a coherent transition radiation mm wave light source", *Infrared Physics and Technology*, vol. 51, pp. 410-412, 2008.